Autism Research

WILEY | INSAR International Society for Autism Research

RESEARCH ARTICLE OPEN ACCESS

Altered Brain Structure in an ATRX-Deficient Mouse Model of Autism Spectrum Disorder

Katherine Quesnel[1,2,3] | Jacob Ellegood[4,5] | Jason P. Lerch[4,5,6] | Nathalie G. Bérubé[1,2,3,7]

[1]Department of Anatomy & Cell Biology, Western University, London, ON, Canada | [2]Department of Paediatrics, Western University, London, ON, Canada | [3]Division of Genetics & Development, Children's Health Research Institute, London, ON, Canada | [4]Mouse Imaging Centre, The Hospital for Sick Children, Toronto, ON, Canada | [5]Department of Medical Biophysics, The University of Toronto, Toronto, ON, Canada | [6]Nuffield Department of Clinical Neuroscience, University of Oxford, Oxford, UK | [7]Department of Oncology, Western University, London, ON, Canada

Correspondence: Nathalie G. Bérubé (nberube@uwo.ca)

Received: 4 July 2025 | **Revised:** 24 January 2026 | **Accepted:** 29 January 2026

Keywords: autism | brain structure | imaging | mice | sex differences

ABSTRACT

Mutations in the *ATRX* gene are a primary cause of alpha-thalassemia intellectual disability X-linked (ATRX) syndrome, which is characterized by intellectual disability, autism, and a range of brain structural abnormalities, including microcephaly. We previously showed that mice with conditional ATRX ablation in forebrain excitatory neurons display deficits in fear memory and autism-related behaviors, with some effects exhibiting sexual dimorphism. In this study, we used high-resolution magnetic resonance imaging (MRI) to systematically characterize brain structural changes associated with these behavioral abnormalities. Whole-brain analysis revealed male-specific microcephaly, while subregional analysis identified significant reductions in hippocampal structures and increased volume of the caudal cortex in mutant animals of both sexes. We also identified structural alterations in regions retaining ATRX expression, such as the thalamus, midbrain, cerebellum, and several fiber tracts. These findings suggest that ATRX loss disrupts the coordinated development of interconnected brain regions. Overall, our results implicate impaired cortico-thalamic-cerebellar connectivity as a potential neural substrate underlying the autistic-like behaviors observed in this mouse model, providing new insights into the neurobiological basis of ATR-X syndrome.

1 | Introduction

Alpha-thalassemia intellectual disability X-linked (ATRX) is a large chromatin remodeling protein crucial for genomic integrity and maintenance of heterochromatin (Bérubé et al. 2000; Gibbons and Higgs 2000). Hypomorphic mutations in *ATRX* are associated with ATR-X syndrome, which is characterized by mild-to-severe intellectual disability (ID) as well as non-syndromic ID. *ATRX* is also classified as a high-risk gene for autism spectrum disorder (ASD). Patients with ATR-X syndrome exhibit global neurodevelopmental delays, skeletal malformations such as short stature and craniofacial alterations, and a portion of patients are reported to have microcephaly (Gibbons et al. 2008; Gibbons and Higgs 2000).

We have previously characterized a mouse model with early embryonic deletion of *Atrx* in excitatory neurons of the forebrain. These mice are viable and survive to adulthood with no obvious health complications or developmental abnormalities noted; however, in some cases, severe repetitive behaviors led to self-injury requiring euthanasia. In this model, both male and female adult mice display fear memory impairments, hyperactivity and repetitive behaviors– a core ASD feature. Additionally, male mice specifically display auditory sensory gating deficits, social memory deficits and social aggression (Quesnel et al. 2023). In humans, females who carry *ATRX* mutations are protected from clinical symptoms due to skewed X-chromosome inactivation that favors the expression of the functional allele (Gibbons et al. 2008). In contrast, in

Lay Summary

Changes in a gene called ATRX are known to affect brain development and are linked to intellectual disability and autism. In our previous work, we found that removing this gene early in brain development caused mice to show behaviors like those seen in people with autism. In this study, we used detailed brain scans to see if these behavioral changes were linked to differences in brain structure. We found that male mice without ATRX had smaller brains and bodies, while female mice did not show the same brain size reduction. However, both male and female mice had smaller areas of the brain important for memory and movement, and larger areas involved in thinking and sensing. We also saw changes in parts of the brain where ATRX was still present, suggesting that early changes in one area can affect how the whole brain develops. These findings help us understand how early disruptions in brain development might lead to autism-related behaviors.

our mouse model, females carry deletions on both X chromosomes and have a full deletion of ATRX (Quesnel et al. 2023). Therefore, this model is more relevant to understanding how total ATRX deficiency contributes to ASD-like phenotypes rather than classical ATR-X syndrome in females. Further characterization of this model will help elucidate the developmental consequences of ATRX loss, including the specific brain structures affected and how these alterations contribute to the ASD features observed.

ASD is highly heterogeneous, both in terms of the phenotypes displayed and the causative genes, many of which are unknown. Some studies have tried to cluster ASD patients according to MRI findings based on neuroanatomical abnormalities relating to their clinical features (Hong et al. 2018; Liu et al. 2022). Investigating mouse models with specific behavioral phenotypes can help directly link brain structural alterations to corresponding behaviors. For instance, a study examining 26 different ASD mouse models found common brain volume changes in regions such as the cerebellar cortex and striatum—areas frequently implicated in human ASD MRI studies (Ellegood et al. 2015). A recent study identified consistent neuroanatomical clusters in both mouse models and human NDD populations, linking brain structure to underlying molecular pathways and highlighting connections between gene interactions, neuroanatomy, and behavioral phenotypes (Ellegood et al. 2025). The cerebellum has been shown to be disrupted in mouse models displaying social deficits (Al Sagheer et al. 2018; Haida et al. 2019), while striatal volume in ASD patients has been correlated with repetitive behaviors (Hollander et al. 2005). In this study, we aim to evaluate volumetric alterations in *Atrx*^{NEXCre} mice that result from Atrx loss during brain development, and correlate our findings with behavioral changes observed in this mouse model, as well as clinical features seen in ASD patients. ATR-X syndrome is rare, with just over 200 reported cases, and exhibits a range of neurodevelopmental phenotypes. An MRI study of 27 ATR-X patients revealed considerable variability in neuroanatomical alterations (Wada et al. 2013). Notably, one patient showed underdevelopment of the cerebellar vermis, and four patients had underdevelopment of the corpus callosum, supporting previous findings that the cerebellum and disrupted connectivity play a role in ASD (Ellegood et al. 2015). Another mouse model with post-natal deletion of *Atrx* in forebrain excitatory neurons displayed alterations in hippocampal regions correlating with memory deficits, but no ASD-features were detected in this model (Martin-Kenny and Bérubé 2020; Tamming et al. 2020). Therefore, comparing our earlier timepoint for *Atrx* deletion with the presence of ASD-features could identify brain regions correlating with memory deficits vs. ASD associated behaviors. Our findings indicate significant reduction in brain size, decreased relative volumes in the hippocampus and cerebellum and their associated fiber tracts, alongside enlargement of caudal cortical subregions, thalamus, and midbrain regions. These results suggest that disruption in cortico-thalamic-cerebellar pathways may contribute to the ASD behaviors characteristic of this mouse model.

2 | Materials and Methods

2.1 | Animal Care and Husbandry

Conditional inactivation of *Atrx* in post-mitotic excitatory neurons was achieved beginning at embryonic day 11.5 (E11.5). To generate experimental animals, 129SV female mice heterozygous for *Atrx*^{loxP} alleles (Berube et al. 2005), were crossed with C57BL/6J male mice expressing Cre recombinase under the control of the NEX-Cre promoter (Goebbels et al. 2006). Male offspring carrying a floxed *Atrx* allele on the X chromosome and the NEX-Cre transgene (*Atrx*^{NEXCre} males) served as knockout animals, while male littermates with a wild-type *Atrx* allele and the NEX-Cre transgene were used as controls to account for any effects of Cre expression. Similarly, homozygous *Atrx* floxed female mice expressing NEX-Cre (*Atrx*^{NEXCre} females) were used as female knockouts, with wild-type *Atrx*, NEX-Cre-positive females serving as controls. Genotyping was performed as previously described (Quesnel et al. 2023).

To generate Cre-reporter mice, Sun1-GFP mice [B6;129-Gt(ROSA)26Sortm5(CAG-Sun1/sfGFP)Nat/J; IMSR JAX:021039; MGI:5614796] (Mo et al. 2015) were crossed with C57BL/6 *Atrx*^{loxP} mice. This cross produced C57BL/6 female offspring heterozygous for both the *Atrx*^{loxP} allele and the Sun1-GFP reporter. These double heterozygous females were then incorporated into the breeding scheme described above to enable tracing of brain regions with Cre-mediated recombination and subsequent *Atrx* ablation. All animal procedures were conducted in accordance with the regulations of the Animals for Research Act of the province of Ontario and approved by the University of Western Ontario Animal Care and Use Committee (protocols 2021-049 and 2021-064). Mice were housed under a 12-h light/12-h dark cycle with ad libitum access to food and water.

2.2 | Immunofluorescence Staining

Mice 3-months of age ($n = 4$) were perfused transcardially with cold 1× PBS, followed by cold 4% paraformaldehyde (PFA). Brains were post-fixed overnight in 4% PFA at 4°C, then washed

in 1× PBS and sunk in 30% sucrose for a minimum of one week. Tissues were embedded in Cryomatrix (Epredia, cat# 6769006) using an ethanol–dry ice slurry and stored at −80°C. Brains were sectioned at 10 μm thickness using a Leica CM3050 S cryostat and mounted onto Superfrost Plus microscope slides (Fisher Scientific, cat# 12-550-15). Sections were rehydrated in 1× PBS and subjected to antigen retrieval by boiling in sodium citrate buffer (pH 6.0, 0.5% Tween-20) for 15 min. Permeabilization was performed with 1× PBS containing 0.03% Triton X-100 for 10 min, followed by blocking for 1 h in 1× PBS with 0.3% Triton X-100 and 5% goat serum. Primary antibodies diluted in blocking solution were applied overnight at 4°C: anti-Atrx (Santa Cruz, sc15408; rabbit, 1:150) and anti-GFP (Invitrogen, PA1-95333; chicken, 1:200). After washing with 1× PBS containing 0.3% Triton X-100, sections were incubated for 1 h at room temperature with the appropriate secondary antibodies (Alexa Fluor 594 anti-rabbit, Thermo Scientific, cat# A11012, 1:1000; Alexa Fluor 488 anti-chicken, Thermo Scientific, cat# A11039, 1:1000). Slides were washed, counterstained with DAPI, rinsed, and coverslipped using ImmunoMount (Thermo Scientific, cat# 9990402). Images were acquired using a Leica CTR 6500 microscope with OpenLab and Velocity software.

2.3 | Brain Histological Analysis

Coronal brain sections were stained with hematoxylin and eosin (H&E) to assess overall brain structure. Sections were first rehydrated in 70% ethanol for 5 min, followed by a 5-min rinse in distilled water. Slides were then immersed in hematoxylin solution for 2 min, rinsed under cold running tap water for 30 s, incubated in Tasha's bluing solution for 30 s, and washed in tap water for 8 min. Sections were subsequently stained with 5% eosin Y for 2 min, followed immediately by two washes in 70% ethanol. Dehydration was performed with a 1-min wash in 90% ethanol, followed by two 2-min washes in 100% ethanol. Sections were then cleared in xylene with three 5-min washes and mounted using Permount Mounting Media (Fisher Chemical, SP15-100). Two weeks post-staining, slides were cleaned and imaged using a Leica Aperio ScanScope. Images were analyzed with ImageScope software. Quantification of total brain area (mm^2) and corpus callosum thickness (mm) was performed using ImageJ software.

2.4 | Magnetic Resonance Ex Vivo Brain Imaging

Mice 10–13 months of age ($Ctrl^{male}$ $n = 10$, $Atrx^{NEXCre\ male}$ $n = 11$, $Ctrl^{female}$ $n = 16$, $Atrx^{NEXCre\ female}$ $n = 12$) were anesthetized with a mixture of ketamine/xylazine and intracardially perfused with 30 mL of 1xPBS containing 0.05 U/mL heparin (Sigma) and 2 mM ProHance (Bracco Diagnostics, a Gadolinium contrast agent) followed by 30 mL of 4% PFA containing 2 mM ProHance (Cahill et al. 2012; Lerch et al. 2011). Perfusions were performed at a rate of approximately 2 mL/min. After perfusion, mice were decapitated and the skin, lower jaw, ears, and the cartilaginous nose tip were removed. The brain and remaining skull structures were incubated in 4% PFA + 2 mM ProHance overnight at 4°C then transferred to 1xPBS containing 2 mM ProHance and 0.02% sodium azide for at least 1 month prior to scanning (de Guzman et al. 2016).

A 7-Tesla 306 mm horizontal bore magnet (BioSpec 70/30 USR, Bruker, Ettlingen, Germany) with a ParaVision 6.0.1 console was used to image brains within their skull. Eight samples were imaged in parallel using a custom-built 8-coil solenoid array. To acquire anatomical images, the following scan parameters were used: T2-weighted 3D fast spin echo (FSE) sequence with a cylindrical acquisition of k-space, TR/TE/ETL = 350 ms/12 ms/6, TEeff = 30 ms, four effective averages, FOV/matrix-size = 20.2 × 20.2 × 25.2 mm/504 × 504 × 630, total-imaging-time = 13.2 h. The resulting anatomical images had an isotropic resolution of 40 μm voxels.

2.5 | Image Registration and Analysis

Registration consisted of both linear (rigid then affine) transformations and non-linear transformations. These registrations were performed with a combination of mni_autoreg tools (Collins et al. 1994) and ANTS (advanced normalization tools) (Avants et al. 2008, 2011). After registration, all scans were resampled with the appropriate transform and averaged to create a population atlas representing the average anatomy of the study sample. The result of these registrations was deformation fields that transform images to a consensus average. Therefore, these deformation fields quantify anatomical differences between images. As detailed in previous studies (Lerch et al. 2008; Nieman et al. 2006), the Jacobian determinants of the deformation fields were computed and analyzed to measure the volume differences between subjects at every voxel. A pre-existing classified MRI atlas was warped onto the population atlas (containing 282 different segmented structures encompassing cortical lobes, large white matter structures such as the corpus callosum, ventricles, cerebellum, brain stem, and olfactory bulbs (Dorr et al. 2008; Qiu et al. 2018; Richards et al. 2011; Steadman et al. 2014; Ullmann et al. 2013)) to compute the volume of brain structures in all the input images. A linear model with a genotype predictor was used to assess significance. The model was either fit to the volume of every structure independently (structure-wise statistics) or fit to every voxel independently (voxel-wise statistics), and multiple comparisons in this study were controlled for using the False Discovery Rate (Genovese et al. 2002). FDR < 0.10 was considered statistically significant.

A complete list of relative volumes and raw MRI absolute volume data used in the current analyses is provided in the Data S1.

3 | Results

3.1 | Sex-Specific Microcephaly and Regional Brain Alterations in *Atrx*^{NEXCre} Mice

Ex vivo MRI analysis of 12-month-old mice revealed significant microcephaly in $Atrx^{NEXCre}$ compared control male mice (FDR = 0.0065), whereas female $Atrx^{NEXCre}$ mice exhibited no global brain volume differences (Figure 1A). This male-specific reduction in brain size parallels the heightened neurological severity observed in the mutant male mice (Quesnel et al. 2023) and aligns with the male predominance of ASD diagnoses. Both male and female $Atrx^{NEXCre}$ mice displayed

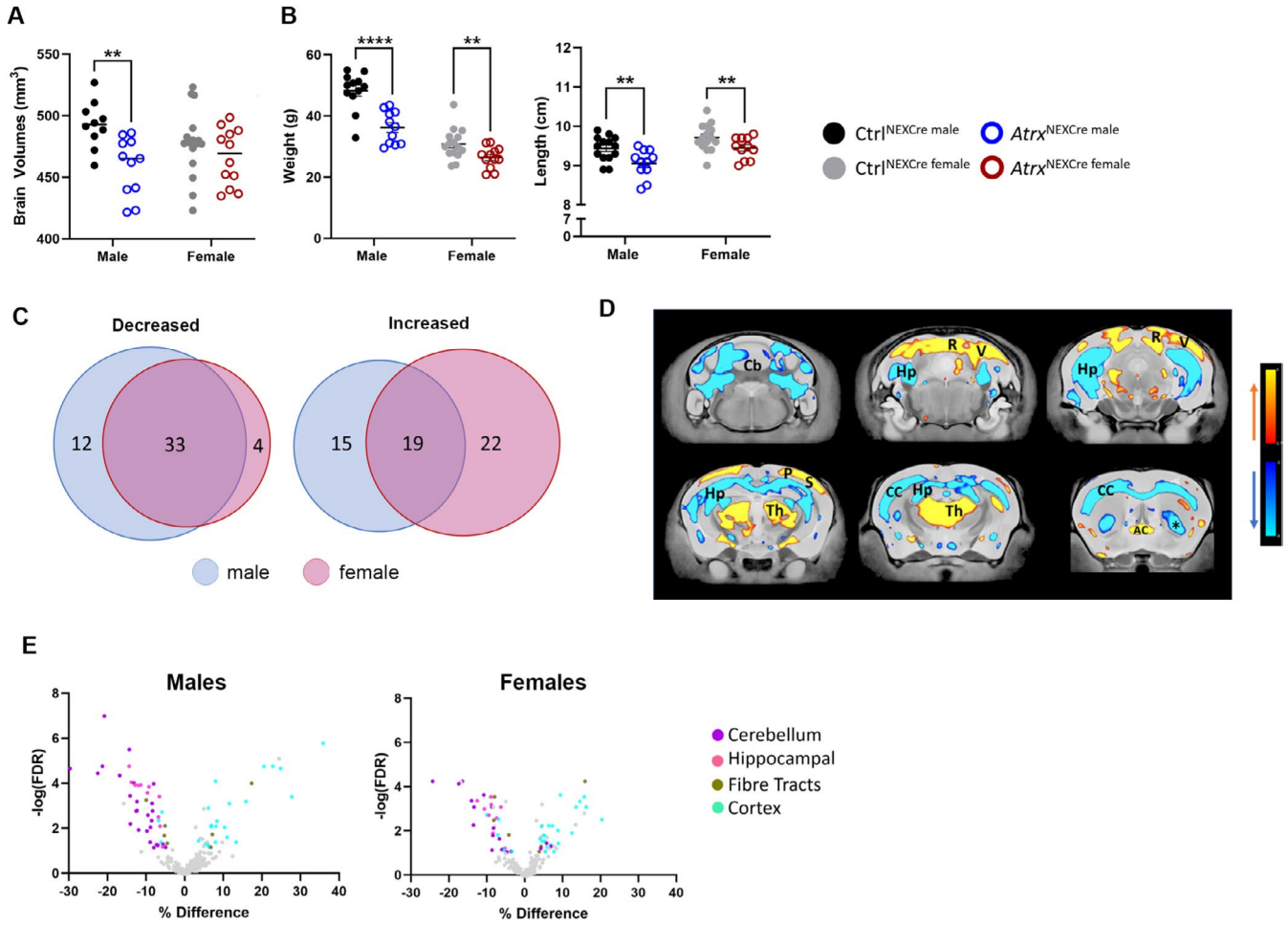

FIGURE 1 | Reproducible regional brain volumetric changes in the *Atrx*^{NEXCre} compared to control mice. (A) Total brain volume and (B) body weight and length of 12-month-old *Atrx*^{NEXCre} and control mice. Total brain volume: **FDR <0.05. Body size: **$p<0.05$, ****$p<0.0001$. (C) Venn diagrams displaying the overlap of brain subregions with significantly altered relative volume in male and female *Atrx*^{NEXCre} mice. (D) Coronal brain images highlight areas with significantly increased (red-yellow spectrum) and decreased (blue spectrum) relative volume. (E) Volcano plot of 188 color-coded significantly changed brain subregions (cerebellum [purple], hippocampus [pink], fiber tracts [gold], cortex [blue]). AC, anterior commissure; Cb, cerebellum; CC, corpus callosum; Hp, Hippocampus; *P*, parietal cortex; *R*, retrosplenial cortex; Th, thalamus; V, visual cortex. *Posterior ventral caudoputamen. Ctrl^{male} $n=10$, *Atrx*$^{NEXCre\ male}$ $n=11$, Ctrl^{female} $n=16$, *Atrx*$^{NEXCre\ female}$ $n=12$.

reduced body size at 12 months, including decreased body weight (males: $p<0.0001$; females: $p=0.0162$) and shorter nose-to-tail length (males: $p=0.0091$; females: $p=0.0426$) (Figure 1B). Brain size strongly correlated with body size in males ($r=0.82$, $p=0.001$) but not in female mutant mice ($r=0.24$, $p=0.38$), suggesting sex-specific mechanisms governing neurodevelopmental scaling.

To account for total brain volume differences, subsequent analyses used relative regional volumes. In males, 45 of 188 brain subregions showed decreased relative (i.e., after normalizing for overall brain size) volume, while 34 exhibited increases (FDR <0.1). Females displayed similar patterns, with 37 subregions decreased and 41 increased (Figure 1C,D). Across both sexes, volume reductions predominated in the cerebellum and hippocampus—regions critical for motor coordination and memory—while expansions occurred primarily in cortical areas. Fiber tracts showed both increased and decreased relative volume (Figure 1E).

3.2 | Ultrastructural Differences in Hippocampal and Cortical Regions

Significant alterations in relative volume were observed in two major forebrain regions—the hippocampus and the cortex—of *Atrx*^{NEXCre} mice. The hippocampal formation exhibited a marked reduction in relative volume in both male (FDR $=0.0028$) and female (FDR $=0.0041$) *Atrx*^{NEXCre} brains compared to controls (Figure 2A). This reduction aligns with previously reported memory deficits in this model, underscoring the functional relevance of these structural changes. Further analysis of hippocampal subregions revealed that the subiculum, CA1, CA2, and CA3 regions were significantly reduced, whereas the dentate gyrus remained unaffected (Figure 2B, Figure S1).

In contrast, the total isocortex displayed a significant increase in relative volume in male *Atrx*^{NEXCre} mice (FDR $=0.0005$), an effect not observed in females (Figure 3A). Subregional analysis of the cortex in males revealed significant increases in the anterior

A

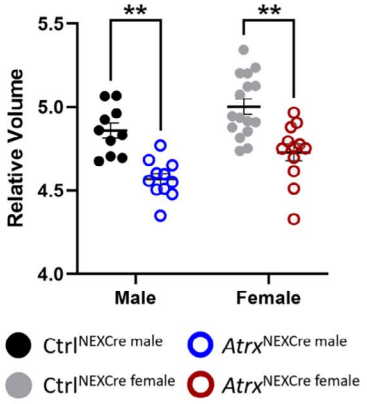

B

Males

	$Atrx^{NEXCre}$		$Cont^{NEXCre}$				
	Mean	SD	Mean	SD	%Diff	Effect	FDR
Retrohippocampal region	3.5995	0.16	3.6737	0.11	-2.02	-0.69	0.3472
Subiculum	**1.0612**	**0.04**	**1.1664**	**0.04**	**-9.02**	**-2.71**	**0.0001***
Entorhinal area	2.5383	0.14	2.5072	0.12	1.24	0.27	0.6721
Hippocampal region	**4.5685**	**0.11**	**4.8587**	**0.14**	**-5.97**	**-2.00**	**0.0004***
Field CA1	**1.7658**	**0.07**	**1.9331**	**0.05**	**-8.65**	**-3.10**	**0.0001***
Field CA2	**0.2379**	**0.01**	**0.2671**	**0.01**	**-10.92**	**-4.66**	**0.0001***
Field CA3	**1.3194**	**0.04**	**1.3804**	**0.05**	**-4.41**	**-1.26**	**0.0157***
Dentate gyrus	1.2454	0.04	1.2782	0.06	-2.57	-0.54	0.2731

Females

	$Atrx^{NEXCre}$		$Cont^{NEXCre}$				
	Mean	SD	Mean	SD	%Diff	Effect	FDR
Retrohippocampal region	3.3061	0.12	3.4277	0.18	-3.55	-0.68	0.1113
Subiculum	**1.0364**	**0.02**	**1.1052**	**0.04**	**-6.23**	**-1.84**	**0.0002***
Entorhinal area	2.2697	0.12	2.3225	0.16	-2.27	-0.33	0.4901
Hippocampal region	**4.7283**	**0.18**	**5.0032**	**0.18**	**-5.49**	**-1.49**	**0.0031***
Field CA1	**1.7988**	**0.08**	**1.9558**	**0.09**	**-8.03**	**-1.73**	**0.0007***
Field CA2	**0.2530**	**0.02**	**0.2699**	**0.02**	**-6.26**	**-1.08**	**0.0378***
Field CA3	**1.4211**	**0.04**	**1.4990**	**0.06**	**-5.19**	**-1.41**	**0.0030***
Dentate gyrus	1.2555	0.06	1.2786	0.05	-1.81	-0.49	0.4011

FIGURE 2 | Significantly decreased relative volume of the hippocampal formation in $Atrx^{NEXCre}$ mice. (A) Decreased relative volume of the hippocampal formation and (B) of specific hippocampal subregions for male and female mice. Blue = significant relative decrease in volume. FDR, false discovery rate; SD, standard deviation. *FDR < 0.1,**FDR < 0.05. $Ctrl^{male}$ $n = 10$, $Atrx^{NEXCre\ male}$ $n = 11$, $Ctrl^{female}$ $n = 16$, $Atrx^{NEXCre\ female}$ $n = 12$.

cingulate, infralimbic, retrosplenial, auditory, posterior parietal association, perirhinal, and visual areas (FDR < 0.1). In female $Atrx^{NEXCre}$ mice, significant increases were observed in the retrosplenial, ectorhinal, posterior parietal association, and visual areas. Conversely, these females exhibited significant decreased volume in the somatomotor, frontal pole, and somatosensory cortical regions (Figure 3B, Figure S2).

The most pronounced increases in relative volume, observed in both sexes, were localized to the retrosplenial cortex (male FDR = 0.0002, female FDR = 0.0032), posterior parietal association area (male FDR = 0.0002, female FDR = 0.0008), and visual cortex (male FDR < 0.0001, female FDR = 0.0001) (Figure 4A). The analysis of subcategories within these areas revealed significant volume increases in cingulate areas 29a and 29b, lateral and medial parietal association areas, the secondary visual cortex, primary visual area, posteromedial visual area, and the anteromedial visual area (Figure 4B).

Collectively, these findings demonstrate that ATRX deficiency leads to distinct and region-specific ultrastructural changes in the hippocampus and cortex, with both shared and sex-specific patterns of alteration.

3.3 | Structural Alterations in Brain Regions Retaining ATRX Expression

In addition to regions with ATRX ablation, we observed significant structural changes in multiple brain areas where ATRX expression is retained. Specifically, $Atrx^{NEXCre}$ mice had significantly enlarged striatum (male FDR = 0.0001, female FDR = 0.0833), thalamus (male FDR = 0.0002, female FDR = 0.0005), and midbrain (male FDR = 0.0418, female FDR = 0.0025) compared to control mice (Figure 5A–C). The hypothalamus was significantly larger only in female $Atrx^{NEXCre}$ mice (FDR = 0.0628), while no significant volume changes were detected in the hindbrain in mice of either sex (Figure 5D–E).

Multiple cerebellar subregions also displayed structural alterations. These included the cerebellar cortex, arbor vitae (white matter), and the deep cerebellar nuclei, which are critical for integrating and relaying cerebellar input and output signals (Figure 6, Figure S3) (de Leon and Das 2023). Notably, the fastigial nucleus showed an increased relative volume in female $Atrx^{NEXCre}$ mice (Figure 6A). Despite these localized increases, total cerebellar volume was significantly reduced in both males (FDR = 0.0005) and females (FDR = 0.0037) (Figure 6B). This reduction was accompanied by alterations in cerebellar fiber tracts: the inferior cerebellar peduncle was significantly decreased in males (FDR = 0.0469), whereas the middle cerebellar peduncle was increased in females (FDR = 0.0618). Importantly, the superior cerebellar peduncle—a major pathway connecting the cerebellum to the midbrain and relaying signals through the dentate nucleus to the ventrolateral thalamic nuclei and red nucleus (de Leon and Das 2023) was significantly decreased in both male (FDR = 0.0001) and female mutant mice (FDR = 0.0003) (Figure 6C). ATRX immunofluorescence analysis of $Atrx^{NEXCre}$; SUN1-GFP Cre reporter brain sections confirmed that all of the aforementioned regions do not express Cre recombinase and maintain ATRX expression (Figure S4). These unexpected structural changes in regions retaining ATRX suggest that ATRX deficiency in the developing forebrain can exert indirect, non-cell-autonomous effects on the morphology of interconnected brain regions.

3.4 | Bidirectional Effects of ATRX Deficiency on Fiber Tracts

In addition to abnormalities in cerebellar-associated fiber tracts, we observed significant alterations in major forebrain fiber tracts

A

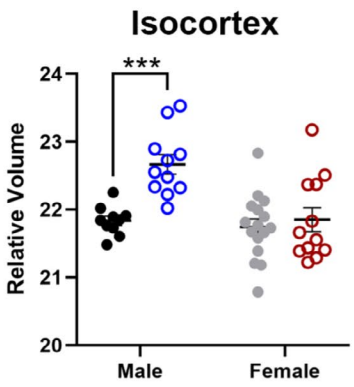

B

Males

	Atrx^{NEXCre}		Ctrl^{NEXCre}				
	Mean	SD	Mean	SD	%Diff	Effect	FDR
Anterior cingulate area	**0.8857**	**0.05**	**0.8392**	**0.03**	**5.54**	**1.38**	**0.0469***
Infralimbic area	**0.1210**	**0.01**	**0.1090**	**0.01**	**10.96**	**1.80**	**0.0249***
Retrosplenial area	**1.3703**	**0.07**	**1.2228**	**0.05**	**12.06**	**3.02**	**0.0002***
Prelimbic area	0.4666	0.04	0.4367	0.03	6.85	1.09	0.1292
Auditory areas	**1.0621**	**0.05**	**1.0097**	**0.04**	**5.20**	**1.20**	**0.0535***
Agranular insular area	0.1619	0.01	0.1690	0.01	-4.25	-0.57	0.2810
Ectorhinal area	2.1397	0.13	2.0363	0.08	5.08	1.26	0.1111
Somatomotor areas	2.7000	0.12	2.7305	0.08	-1.12	-0.40	0.5880
Frontal pole, cerebral cortex	1.3995	0.16	1.3705	0.07	2.11	0.41	0.6721
Orbital area	1.4505	0.07	1.3970	0.04	3.83	1.27	0.1285
Posterior parietal association areas	**0.6260**	**0.03**	**0.5235**	**0.02**	**19.60**	**4.88**	**0.0000***
Perirhinal area	**0.5769**	**0.03**	**0.5436**	**0.03**	**6.11**	**1.00**	**0.0575***
Somatosensory areas	6.8519	0.20	6.8187	0.15	0.49	0.22	0.7426
Temporal association areas	0.6239	0.04	0.5939	0.02	5.05	1.23	0.1245
Visual areas	**2.2300**	**0.10**	**2.0335**	**0.04**	**9.66**	**4.40**	**0.0002***

Females

	Atrx^{NEXCre}		Ctrl^{NEXCre}				
	Mean	SD	Mean	SD	%Diff	Effect	FDR
Anterior cingulate area	0.7891	0.04	0.8026	0.09	-1.68	-0.15	0.7455
Infralimbic area	0.1155	0.01	0.1131	0.01	2.16	0.42	0.4185
Retrosplenial area	**1.3329**	**0.05**	**1.2344**	**0.07**	**7.98**	**1.33**	**0.0032***
Prelimbic area	0.4115	0.03	0.4137	0.04	-0.53	-0.05	0.9076
Auditory areas	0.9975	0.04	0.9945	0.04	0.30	0.07	0.8847
Agranular insular area	0.1639	0.01	0.1702	0.01	-3.73	-0.49	0.2572
Ectorhinal area	**2.1550**	**0.11**	**2.0628**	**0.05**	**4.47**	**1.86**	**0.0231***
Somatomotor areas	**2.6154**	**0.10**	**2.7156**	**0.11**	**-3.69**	**-0.90**	**0.0563***
Frontal pole, cerebral cortex	**1.3181**	**0.11**	**1.3933**	**0.07**	**-5.40**	**-1.09**	**0.0751***
Orbital area	1.4104	0.08	1.3940	0.06	1.17	0.29	0.6666
Posterior parietal association areas	**0.6171**	**0.03**	**0.5423**	**0.03**	**13.80**	**2.26**	**0.0001***
Perirhinal area	0.5420	0.03	0.5259	0.03	3.07	0.54	0.2650
Somatosensory areas	**6.6371**	**0.21**	**6.7982**	**0.19**	**-2.37**	**-0.85**	**0.0926***
Temporal association areas	0.5769	0.03	0.5847	0.03	-1.33	-0.28	0.6285
Visual areas	**2.1685**	**0.10**	**1.9980**	**0.09**	**8.54**	**1.81**	**0.0008***

FIGURE 3 | Legend on next page.

FIGURE 3 | Deletion of ATRX in forebrain excitatory neurons results in relative volume changes in cortical subregions. Tables displaying relative volumes in male and female *Atrx*^{NEXCre} cortical subregions; regions with significantly increased volumes are in orange and significantly decreased volumes are in blue. FDR, false discovery rate; SD, standard deviation. *FDR < 0.1, **FDR < 0.001. Ctrl^{male} $n = 10$, *Atrx*$^{NEXCre\ male}$ $n = 11$, Ctrl^{female} $n = 16$, *Atrx*$^{NEXCre\ female}$ $n = 12$.

in *Atrx*^{NEXCre} mice. The corpus callosum, a critical structure for interhemispheric communication, showed a significant reduction in relative volume in both male (FDR = 0.0006) and female (FDR = 0.0033) *Atrx*^{NEXCre} mice compared to controls. Similarly, the fornix system, which is essential for hippocampal connectivity, was significantly reduced in both males (FDR = 0.0046) and females (FDR = 0.0057) (Figure 7A,B). However, not all fiber tracts were reduced in volume. The temporal limb of the anterior commissure exhibited a significant increase in relative volume in males (FDR = 0.0187), while the olfactory limb of the anterior commissure was significantly increased in both sexes (male FDR = 0.0001, female FDR = 0.0001). Additionally, the posterior commissure showed an increased volume in females (FDR = 0.0867) (Figure 7C–E). Histological analysis further supported these findings. Examination of brain sections confirmed a significant reduction in the thickness of the corpus callosum at 3 months in both sexes (Figure 7F). Collectively, these results demonstrate that ATRX deficiency leads to widespread alterations in structural connectivity, affecting both commissural and projection fiber tracts. The observed changes are largely consistent across sexes, suggesting a fundamental role for ATRX in the development and maintenance of neural connectivity.

4 | Discussion

Our study demonstrates that the loss of ATRX in forebrain excitatory neurons leads to widespread and region-specific structural alterations in the mouse brain. Both male and female *Atrx*^{NEXCre} mice exhibit increased relative volumes in caudal cortical regions, as well as in the thalamus, striatum, and midbrain. At the same time, these mice show reduced volumes in the hippocampus, cerebellum, and associated fiber tracts (Figure 8A). These findings suggest that ATRX deficiency disrupts not only specific brain regions but also global neural connectivity, which may underlie the cognitive and autism-related behaviors observed in this model. It is important to note that the mice used in this study were older adults (10–13 months of age). As mice progress from young to middle and older age, there is evidence for age-related changes in brain structure detectable by MRI, alongside proteomic alterations which impact behavior (Clifford et al. 2023; Tsumagari et al. 2023). Therefore, some of the differences observed in this study could, in part, reflect age-related or hormonal effects. Future work will be needed to investigate the consequences of ATRX loss on brain structure at earlier timepoints to distinguish developmental from aging-related effects.

MRI analysis revealed that male *Atrx*^{NEXCre} mice have reduced brain size correlating to a decrease in body size. Although mutant mice of both sexes displayed reduced body size, only males exhibited a significant reduction in total brain volume. This pattern suggests a sex-dependent vulnerability to ATRX loss. The underlying cause of these growth differences remains unclear, but similar findings have been reported in other mouse models with ATRX deletion in the central nervous system (Tamming et al. 2017, 2020). The reduced hippocampal volume and fornix observed in *Atrx*^{NEXCre} mice are consistent with memory and cognitive deficits, which are also reported in both this mouse model and ATR-X syndrome (Gibbons and Higgs 2000; Quesnel et al. 2023). These findings are similar to those seen in other mouse models with cognitive deficits, including models with mutations in *Nlgn3*, an ASD-associated gene encoding a synaptic adhesion protein, and *MeCP2*, a gene encoding a chromatin remodeling protein associated with Rett syndrome (Akaba et al. 2022; Anand and Dhikav 2012; Ellegood et al. 2011, 2025). However, since models with postnatal *Atrx* deletion show hippocampal deficits without autism features (Quesnel et al. 2023; Martin-Kenny and Bérubé 2020), these changes may be more closely linked to ID than to autism itself.

Our analysis also reveals significantly increased volumes in the retrosplenial, posterior parietal, and visual cortical areas of the caudal cortex in *Atrx*^{NEXCre} mice. In contrast, reductions in these same regions have been reported in ASD mouse models with MeCP2 or *Chd7* mutations, suggesting that volumetric alterations in these cortical areas are linked to ASD-associated behaviors (Akaba et al. 2022; Donovan et al. 2023). The retrosplenial cortex has been implicated in social memory deficits and repetitive behaviors (Garrido et al. 2022; Ha et al. 2015; Thakkar et al. 2008), while the posterior parietal cortex is involved in spatial awareness and working memory (Hahn et al. 2018; Sack 2009). Consistent with these roles, *Atrx*^{NEXCre} mice display cognitive and social memory deficits, as well as repetitive behaviors (Quesnel et al. 2023). These results suggest that structural changes in these caudal cortical regions may contribute directly to the behavioral phenotypes observed with ATRX deficiency.

Alterations in the visual cortex are frequently associated with sensory processing deficits in ASD, including difficulties interpreting visual cues such as facial expressions and body language. Although visual processing has not yet been specifically assessed in *Atrx*^{NEXCre} mice, MeCP2—a chromatin-associated protein that interacts with ATRX—modulates visual cortical neuron activity, and its loss reduces visual activity in mice (Chung and Son 2020; Zhang et al. 2017). We also observed sex-specific differences in cortical structure. For example, males showed increased auditory cortex volume and related sensory processing deficits, such as increased auditory startle response and impaired auditory sensory gating, which were not observed in female mice (Quesnel et al. 2023). These results indicate that structural changes in sensory regions may underlie sex differences in autism-related behaviors, consistent with clinical observations of ASD.

Sex differences are well documented in ASD, with males diagnosed more frequently than females, although the biological mechanisms underlying this disparity remain poorly understood. Factors such as sex chromosomes, X-linked

A

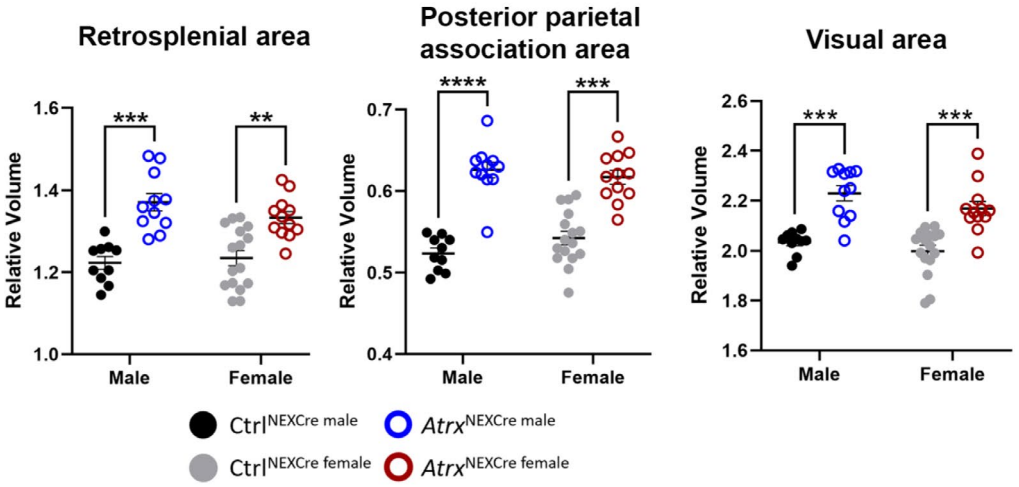

B

Males

	Atrx^{NEXCre}		Ctrl^{NEXCre}				
	Mean	SD	Mean	SD	%Diff	Effect	FDR
Retrosplenial area	1.3703	0.07	1.2228	0.05	12.06	3.02	0.0002*
Retrosplenial area, ventral part	0.6772	0.04	0.6017	0.03	12.54	2.45	0.0005*
Cingulate cortex: area 29a	0.1860	0.01	0.1514	0.01	22.86	3.51	<0.0001*
Cingulate cortex: area 29b	0.1041	0.01	0.0767	0.01	35.86	4.11	<0.0001*
Cingulate cortex: area 29c	0.3870	0.03	0.3737	0.02	3.58	0.60	0.3784
Retrosplenial area, dorsal part	0.6931	0.04	0.6211	0.03	11.59	2.75	0.0008*
Posterior parietal association areas	0.6260	0.03	0.5235	0.02	19.60	4.88	<0.0001*
Lateral parietal association cortex	0.0688	0.01	0.0607	0.01	13.35	1.20	0.0418*
Medial parietal association cortex	0.1259	0.01	0.1009	0.01	24.84	4.42	<0.0001*
Parietal cortex post area rostral part	0.0266	0.00	0.0261	0.00	1.89	0.22	0.6721
*Secondary visual cortex	0.4048	0.03	0.3359	0.02	20.53	4.26	<0.0001*
Visual areas	2.2300	0.10	2.0335	0.04	9.66	4.40	0.0002*
Primary visual area	0.5435	0.04	0.4690	0.02	15.87	3.20	0.0007*
Lateral visual area	0.4292	0.03	0.4352	0.02	-1.39	-0.32	0.6355
posteromedial visual area	0.3882	0.02	0.3591	0.01	8.09	3.21	0.0081*
Anterolateral visual area	0.6278	0.02	0.5812	0.02	8.02	3.03	0.0001*

Females

	Atrx^{NEXCre}		Ctrl^{NEXCre}				
	Mean	SD	Mean	SD	%Diff	Effect	FDR
Retrosplenial area	1.3329	0.05	1.2344	0.07	7.98	1.33	0.0032*
Retrosplenial area, ventral part	0.6301	0.03	0.5884	0.04	7.09	1.13	0.0122*
Cingulate cortex: area 29a	0.1719	0.01	0.1529	0.02	12.44	1.21	0.0127*
Cingulate cortex: area 29b	0.0975	0.01	0.0810	0.01	20.35	1.40	0.0031*
Cingulate cortex: area 29c	0.3607	0.02	0.3545	0.02	1.75	0.26	0.6434
Retrosplenial area, dorsal part	0.7027	0.03	0.6459	0.05	8.79	1.07	0.0096*
Posterior parietal association areas	0.6171	0.03	0.5423	0.03	13.80	2.26	0.0001*
Lateral parietal association cortex	0.0693	0.01	0.0636	0.00	8.85	1.19	0.0373*
Medial parietal association cortex	0.1260	0.01	0.1084	0.01	16.21	2.15	0.0009*
Parietal cortex post area rostral part	0.0261	0.00	0.0247	0.00	5.50	0.72	0.0867*
*Secondary visual cortex	0.3957	0.02	0.3454	0.03	14.56	1.70	0.0005*
Visual areas	2.1685	0.10	1.9980	0.09	8.54	1.81	0.0008*
Primary visual area	0.5304	0.04	0.4584	0.03	15.72	2.32	0.0003*
Lateral visual area	0.4247	0.02	0.4190	0.02	1.36	0.28	0.6099
posteromedial visual area	0.3738	0.03	0.3496	0.02	6.92	1.28	0.0424*
Anterolateral visual area	0.6185	0.03	0.5762	0.03	7.33	1.42	0.0060*

* mediomedial area

FIGURE 4 | Legend on next page.

FIGURE 4 | Most enlarged cortical regions in *Atrx*^{NEXCre} mice. (A) Relative volumes of the most significantly increased isocortex subregions in male and female *Atrx*^{NEXCre} mice. (B) Tables with breakdown of the retrosplenial, posterior parietal association, and visual area subregions in male and female mice. Orange = regions with significantly increased volume. FDR, false discovery rate; SD, standard deviation. *FDR < 0.1, **FDR < 0.05, ***FDR < 0.001, ****FDR < 0.0001. Ctrl^{male} $n = 10$, *Atrx*$^{NEXCre\ male}$ $n = 11$, Ctrl^{female} $n = 16$, *Atrx*$^{NEXCre\ female}$ $n = 12$.

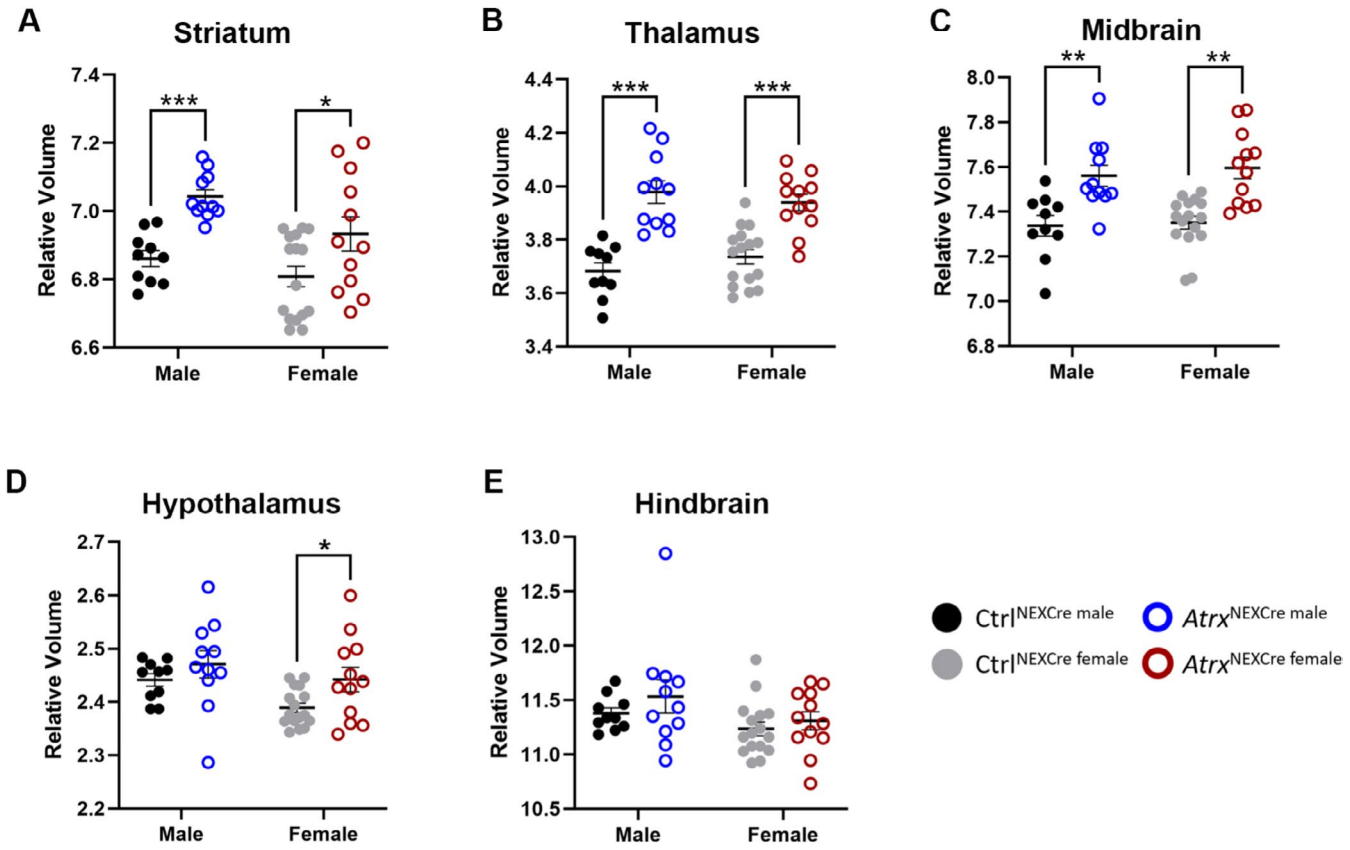

FIGURE 5 | Relative volumetric changes in brain regions that retain ATRX expression in *Atrx*^{NEXCre} mice. Graphs displaying relative brain volumes of (A) Striatum, (B) Thalamus, (C) Midbrain, (D) Hypothalamus, and (E) Hindbrain regions in male and female mice. Ctrl^{male} $n = 10$, *Atrx*$^{NEXCre\ male}$ $n = 11$, Ctrl^{female} $n = 16$, *Atrx*$^{NEXCre\ female}$ $n = 12$. *FDR < 0.10, **FDR < 0.05, ***FDR < 0.001.

gene expression, and sex hormone signaling have been proposed to contribute to differential susceptibility or protective effects across sexes (Ellingford et al. 2024; Jung et al. 2018; Singh et al. 2019). Several theories have been put forward to explain these differences, including the extreme male brain theory, which proposes that ASD represents an exaggeration of typical male neurocognitive patterns; the female protection model, which suggests that females require a higher mutational burden or environmental load to exhibit ASD symptoms; and the female autism phenotype theory, which proposes that females present ASD differently than males and may be underdiagnosed due to diagnostic tools biased toward male-typical symptom profiles (Napolitano et al. 2022). Within this context, the sex-specific structural alterations observed in *Atrx*^{NEXCre} mice, such as the male-specific increase in auditory cortex volume and the female-specific increases in hypothalamic and fastigial nucleus volume, may reflect compensatory or alternative neurodevelopmental pathways that are potentially shaped by ATRX regulation of X-linked genes. Although the functional implications of these differences remain to be determined, they are consistent with the broader idea that ASD-related phenotypes may arise through distinct neurodevelopmental trajectories in males and females (Napolitano et al. 2022). Future studies examining neuronal activity, connectivity, and gene expression in these regions will be important for clarifying how these sex-specific structural differences contribute to divergent sensory and behavioral outcomes.

Interestingly, we identified structural alterations in brain regions that retain ATRX expression, indicating that ATRX deficiency in forebrain excitatory neurons can have non-cell-autonomous effects, potentially through disrupted connectivity or altered developmental signaling. The regional pattern of ATRX loss observed in *Atrx*^{NEXCre} mice corresponds closely with NEX-Cre expression, with pronounced depletion in cortical and hippocampal neurons, as previously reported (Quesnel et al. 2023). In contrast, we observed retention of ATRX in subcortical regions, including the thalamus, striatum, midbrain, and cerebellum. The direction of volumetric change does not correlate with the expression pattern of ATRX. Among regions showing loss of ATRX, the cortex

A

Males

	Atrx^{NEXCre}		Ctrl^{NEXCre}				
	Mean	SD	Mean	SD	%Diff	Effect	FDR
Cerebellar cortex	9.4988	0.42	10.3015	0.33	-7.79	-2.45	0.0007*
Vermal regions	4.1423	0.18	4.4018	0.17	-5.89	-1.54	0.0104*
Hemispheric regions	5.3565	0.25	5.8997	0.19	-9.21	-2.87	0.0002*
Cerebellar nuclei	0.3086	0.02	0.3453	0.01	-10.62	-2.85	0.0001*
Dentate nucleus	0.0740	0.00	0.0934	0.00	-20.80	-4.57	<0.0001*
Interposed nucleus	0.1045	0.01	0.1256	0.01	-16.85	-3.40	<0.0001*
Fastigial nucleus	0.1302	0.01	0.1262	0.01	3.12	0.76	0.2535
Arbor vitae	2.1702	0.09	2.3735	0.05	-8.57	-4.10	0.0001*

Females

	Atrx^{NEXCre}		Ctrl^{NEXCre}				
	Mean	SD	Mean	SD	%Diff	Effect	FDR
Cerebellar cortex	10.2662	0.32	10.7512	0.35	-4.51	-1.38	0.0045*
Vermal regions	4.5050	0.13	4.5922	0.19	-1.90	-0.46	0.2957
Hemispheric regions	5.7611	0.20	6.1589	0.19	-6.46	-2.15	0.0003*
Cerebellar nuclei	0.3150	0.02	0.3390	0.02	-7.07	-1.46	0.0144*
Dentate nucleus	0.0762	0.01	0.0912	0.00	-16.45	-3.06	0.0001*
Interposed nucleus	0.1052	0.01	0.1214	0.01	-13.38	-2.14	0.0008*
Fastigial nucleus	0.1336	0.01	0.1263	0.01	5.75	1.08	0.0363*
Arbor vitae	2.3516	0.15	2.4753	0.15	-5.00	-0.85	0.0843*

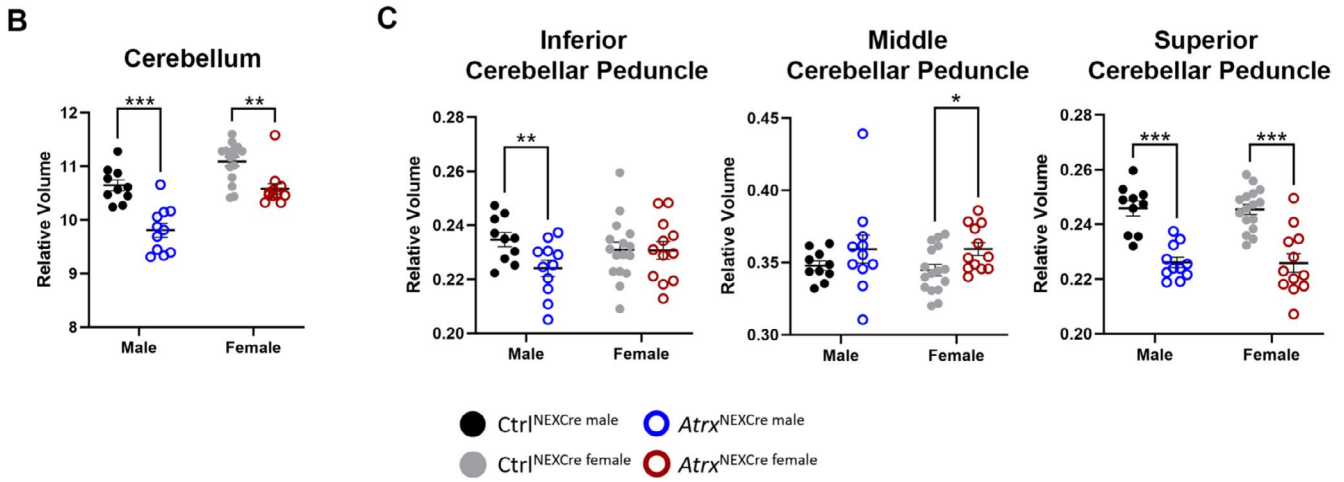

FIGURE 6 | Decreased relative volume of the cerebellum and cerebellar fiber tracts. (A) Table displaying decrease in the relative brain volume of cerebellum subregions; orange = regions with significantly relative increase in volume and blue = significant relative decrease in volume. FDR, false discovery rate; SD, standard deviation. Graph displaying relative volume changes in (B) total cerebellum and (C) cerebellar peduncles in *Atrx*^{NEXCre} mice. Ctrl^{male} $n = 10$, *Atrx*$^{NEXCre\ male}$ $n = 11$, Ctrl^{female} $n = 16$, *Atrx*$^{NEXCre\ female}$ $n = 12$. *FDR < 0.10, **FDR < 0.05, ***FDR < 0.001.

displayed an increase in relative volume, whereas the hippocampus exhibited a reduction. Conversely, among regions retaining ATRX, the striatum, midbrain and thalamus showed relative increases in volume, while the cerebellum decreased in volume. These findings suggest that both direct effects of ATRX loss and indirect, non-cell-autonomous influences on interconnected brain regions contribute to the neuroanatomical phenotype. Alterations in major fiber tracts, including the corpus callosum and fornix, further highlight disrupted connectivity in *Atrx*^{NEXCre} mice.

Our findings support the idea that cerebellar alterations could underlie ASD behaviors. The cerebellum has functional connectivity to the cortex, hippocampus, and amygdala, and is important for cognitive and emotional function. Defects in cerebellar structures are reported in neurodevelopmental disorders, including ASD, ADHD, and ID (Mapelli et al. 2022; Sathyanesan et al. 2019). In addition, pediatric patients with cerebellar lesions often exhibit ID and ASD symptoms, including language deficits, repetitive behaviors, and decreased sociability (Hampson and Blatt 2015). The cerebellum has extensive "closed-loop" connections, forming specific circuits with regions of the cortex and may act as an integrative processor for input and output responses (Courchesne et al. 2007; D'Mello and Stoodley 2015). The most significant reduction in relative brain volume in *Atrx*^{NEXCre} mice was observed in the dentate nucleus, a deep cerebellar

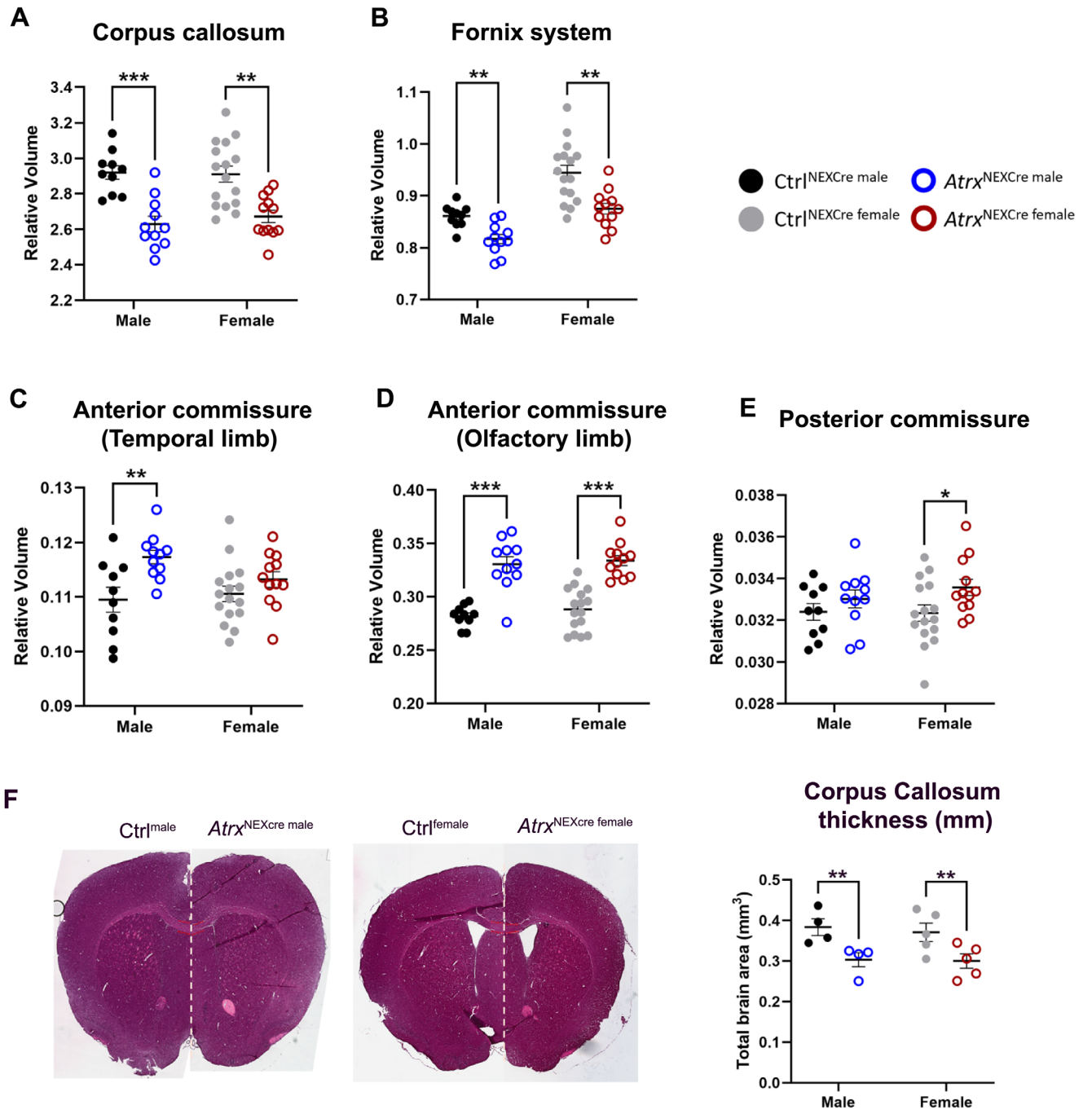

FIGURE 7 | Bimodel effects of ATRX loss on fiber tracts. Graphs displaying decrease in the relative brain volume of (A) corpus callosum and (B) fornix system. Increased relative volume of (C) anterior commissure temporal limb, (D) olfactory limb, and (E) posterior commissure. $Ctrl^{male}$ $n = 10$, $Atrx^{NEXCre\ male}$ $n = 11$, $Ctrl^{female}$ $n = 16$, $Atrx^{NEXCre\ female}$ $n = 12$. *FDR < 0.10, **FDR < 0.05, ***FDR < 0.001. (F) Measurement of corpus callosum thickness (mm) in histological sections at 3-months (Male $n = 4$, Female $n = 5$). **$p < 0.05$.

nucleus involved in connecting the cerebellum with the forebrain, a finding also seen in many other ASD mouse models (Ellegood et al. 2015). The superior cerebellar peduncle, which projects out of the cerebellum through the dentate nucleus to the midbrain and thalamus, also exhibited a significant reduction in relative volume in $Atrx^{NEXCre}$ mice (Hampson and Blatt 2015; de Leon and Das 2023). A previous study in mice demonstrated that disruption of cortico-thalamic-cerebellar connectivity results in ASD features (Kelly et al. 2020). Taken together, the alterations in relative volumes identified in $Atrx^{NEXCre}$ mice are consistent with aberrant cortical-thalamic-cerebellar connectivity.

Early fiber tract alterations in individuals with ASD have been proposed to contribute to the atypical development of brain connectivity (Ha et al. 2015). In this study, MRI data revealed a reduced volume of the corpus callosum in $Atrx^{NEXCre}$ mice, a hallmark in the brains of individuals with ASD and schizophrenia (Domínguez-Iturza et al. 2019; Saxena et al. 2012) and ASD/ID mouse models (Akaba et al. 2022; Donovan et al. 2023; Ellegood et al. 2011). Theories of structural covariance suggest that brain regions are both structurally and functionally connected, potentially due to coordinated growth driven by the expression of shared gene sets during development. The

A)

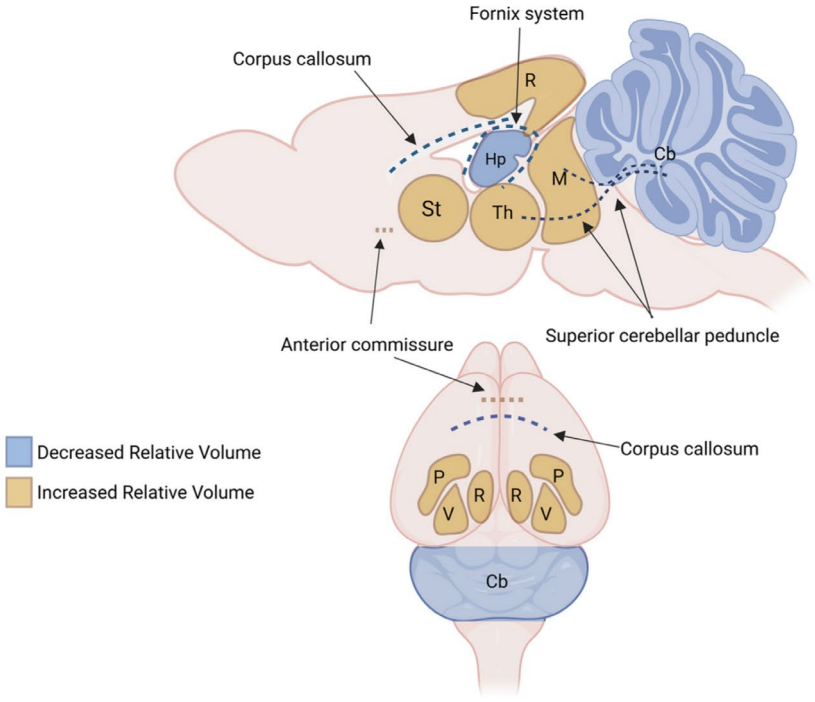

B)

Brain Region/ Fibre Tract	Volumetric change in *Atrx*^{NEXCre} mice	Behavioral phenotype in *Atrx*^{NEXCre} mice	Clinical feature in ASD
Hippocampus	↓	• Deficits in fear and social memory	• Learning/memory deficits (not ASD specific phenotype)
Cerebellum	↓	• Increased grooming (repetitive behaviour)	• Language deficits, • Repetitive behaviors & stereotypies • Decreased sociability
Retrosplenial cortical area	↑	• Decreased social memory • Increased grooming (repetitive behaviour)	• Social memory • Repetitive behaviours & stereotypies
Posterior parietal cortical area	↑	• Unable to assess*	• Spatial and working memory
Visual cortex	↑	• Not assessed	• Visual sensory processing (difficulty interpreting facial cues)
Auditory cortex	↑**	• Increased startle response** • Auditory sensory gating deficits**	• Auditory sensory processing

**Attempts to assess working memory using the Y-maze were unsuccessful because Atrx^{NEXCre} mice repeatedly jumped out of the apparatus. Similarly, efforts to evaluate spatial memory using the Morris water maze were limited, as the mice refused to swim.*
***male specific (Quesnel et al., 2023)*

FIGURE 8 | Legend on next page.

FIGURE 8 | Summary of relative brain volume changes in *Atrx*^{NEXCre} mice. (A) Schematic depicting relative brain volume changes shared by male and female *Atrx*^{NEXCre} mice. (B) Table summarizing volumetric changes, corresponding to behavioral outcomes previously observed and clinical features of ASD. Cb, cerebellum; Hp, hippocampus; M, midbrain; *P*, posterior parietal area; *R*, retrosplenial area; St, striatum; Th, thalamus; V, visual area.

cortical-thalamic relay of information through structural and functional connection is an example of structural covariance (Yee et al. 2024). Disruption of developmental gene expression patterns due to loss of ATRX in forebrain excitatory neurons could lead to alterations in both structural connectivity and the gene expression profiles required for the growth and maturation of subcortical regions such as the thalamus and striatum. Previous work examining *Atrx*^{NEXCre} mice at P20 found no differences in myelin-associated proteins (MAG, MOG, or MBP) by immunostaining or western blot, suggesting that the establishment of myelination proceeds normally in this model (Rowland et al. 2023). However, because these assessments were performed at postnatal day 20, it remains possible that myelin maintenance or aging-related changes in white matter are impacted due to loss of ATRX leading to the changes in fiber tract volumes observed in this study. Further investigation is needed to characterize the specific gene expression changes in *Atrx*^{NEXCre} mice during development and how these alterations might contribute to impaired subcortical development.

This study is limited by its focus on volumetric MRI, which cannot directly assess functional or structural connectivity. Future work using functional MRI and diffusion tensor imaging will be important to clarify the impact of ATRX loss on brain networks. Additionally, examining these changes across development could identify critical periods for intervention. Further investigation into the mechanisms driving regional volume increases, particularly in sensory cortices, may provide insight into sex-specific sensory processing deficits in ASD and inform future therapeutic strategies.

In summary, our findings highlight the essential role of ATRX in shaping brain structure and connectivity. The observed alterations in cortical, hippocampal, cerebellar, and subcortical regions in *Atrx*^{NEXCre} mice mirror key features of ASD and ID. Figure 8B summarizes the structural changes in *Atrx*^{NEXCre} mice and their correspondence to the behavioral phenotypes previously reported in this model (Quesnel et al. 2023), as well as to clinical features reported in ASD. These results support the use of this model to study the neural basis of autism and related neurodevelopmental disorders.

Author Contributions

K.Q. contributed to conceptualization, design and execution of experiments, data interpretation, and writing of article. J.E. and J.P.L. contributed to execution of experiments, data analysis, and manuscript editing. N.G.B. contributed the conception, design, interpretation of data, and writing of article.

Funding

K.Q. was the recipient of an Ontario Graduate Scholarship, a graduate studentship from the Department of Pediatrics at Western University, and the Sir Fredrick Banting CIHR Doctoral Award. This work was supported by operating funds from the Canadian Institutes for Health Research to N.G.B. (FRN# 178329).

Ethics Statement

The authors have nothing to report.

Conflicts of Interest

The authors declare no conflicts of interest.

Data Availability Statement

The data that supports the findings of this study are available in the Supporting Information of this article.

References

Akaba, Y., T. Shiohama, Y. Komaki, et al. 2022. "Comprehensive Volumetric Analysis of Mecp2-Null Mouse Model for Rett Syndrome by T2-Weighted 3D Magnetic Resonance Imaging." *Frontiers in Neuroscience* 16: 885335. https://doi.org/10.3389/fnins.2022.885335.

Al Sagheer, T., O. Haida, A. Balbous, et al. 2018. "Motor Impairments Correlate With Social Deficits and Restricted Neuronal Loss in an Environmental Model of Autism." *International Journal of Neuropsychopharmacology* 21, no. 9: 871–882. https://doi.org/10.1093/ijnp/pyy043.

Anand, K., and V. Dhikav. 2012. "Hippocampus in Health and Disease: An Overview." *Annals of Indian Academy of Neurology* 15, no. 4: 239–246. https://doi.org/10.4103/0972-2327.104323.

Avants, B. B., C. L. Epstein, M. Grossman, and J. C. Gee. 2008. "Symmetric Diffeomorphic Image Registration With Cross-Correlation: Evaluating Automated Labeling of Elderly and Neurodegenerative Brain." *Medical Image Analysis* 12, no. 1: 26–41. https://doi.org/10.1016/j.media.2007.06.004.

Avants, B. B., N. J. Tustison, G. Song, P. A. Cook, A. Klein, and J. C. Gee. 2011. "A Reproducible Evaluation of ANTs Similarity Metric Performance in Brain Image Registration." *NeuroImage* 54, no. 3: 2033–2044. https://doi.org/10.1016/j.neuroimage.2010.09.025.

Berube, N. G., M. Mangelsdorf, M. Jagla, et al. 2005. "The Chromatin-Remodeling Protein ATRX Is Critical for Neuronal Survival During Corticogenesis." *Journal of Clinical Investigation* 115, no. 2: 258–267. https://doi.org/10.1172/JCI22329.

Bérubé, N. G., C. A. Smeenk, and D. J. Picketts. 2000. "Cell Cycle-Dependent Phosphorylation of the ATRX Protein Correlates With Changes in Nuclear Matrix and Chromatin Association." *Human Molecular Genetics* 9, no. 4: 539–547. https://doi.org/10.1093/hmg/9.4.539.

Cahill, L. S., C. L. Laliberté, J. Ellegood, et al. 2012. "Preparation of Fixed Mouse Brains for MRI." *NeuroImage* 60, no. 2: 933–939. https://doi.org/10.1016/j.neuroimage.2012.01.100.

Chung, S., and J. W. Son. 2020. "Visual Perception in Autism Spectrum Disorder: A Review of Neuroimaging Studies." *Journal of the Korean Academy of Child and Adolescent Psychiatry* 31, no. 3: 105–120. https://doi.org/10.5765/jkacap.200018.

Clifford, K. P., A. E. Miles, T. D. Prevot, et al. 2023. "Brain Structure and Working Memory Adaptations Associated With Maturation and Aging in Mice." *Frontiers in Aging Neuroscience* 15: 1195748. https://doi.org/10.3389/fnagi.2023.1195748.

Collins, D. L., P. Neelin, T. M. Peters, and A. C. Evans. 1994. "Automatic 3D Intersubject Registration of MR Volumetric Data in Standardized Talairach Space." *Journal of Computer Assisted Tomography* 18, no. 2: 192–205. https://doi.org/10.1097/00004728-199403000-00005.

Courchesne, E., K. Pierce, C. M. Schumann, et al. 2007. "Mapping Early Brain Development in Autism." *Neuron* 56, no. 2: 399–413. https://doi.org/10.1016/j.neuron.2007.10.016.

de Guzman, A. E., M. D. Wong, J. A. Gleave, and B. J. Nieman. 2016. "Variations in Post-Perfusion Immersion Fixation and Storage Alter MRI Measurements of Mouse Brain Morphometry." *NeuroImage* 142: 687–695. https://doi.org/10.1016/j.neuroimage.2016.06.028.

de Leon, A. S., and J. M. Das. 2023. "Neuroanatomy, Dentate Nucleus."In *StatPearls*. StatPearls Publishing.

D'Mello, A. M., and C. J. Stoodley. 2015. "Cerebro-Cerebellar Circuits in Autism Spectrum Disorder." *Frontiers in Neuroscience* 9: 408. https://doi.org/10.3389/fnins.2015.00408.

Domínguez-Iturza, N., A. C. Lo, D. Shah, et al. 2019. "The Autism- and Schizophrenia-Associated Protein CYFIP1 Regulates Bilateral Brain Connectivity and Behaviour." *Nature Communications* 10, no. 1: 3454. https://doi.org/10.1038/s41467-019-11203-y.

Donovan, A. P. A., L. Rosko, J. Ellegood, et al. 2023. "Pervasive Cortical and White Matter Anomalies in a Mouse Model for CHARGE Syndrome." *Journal of Anatomy* 243, no. 1: 51–65. https://doi.org/10.1111/joa.13856.

Dorr, A. E., J. P. Lerch, S. Spring, N. Kabani, and R. M. Henkelman. 2008. "High Resolution Three-Dimensional Brain Atlas Using an Average Magnetic Resonance Image of 40 Adult C57Bl/6J Mice." *NeuroImage* 42, no. 1: 60–69. https://doi.org/10.1016/j.neuroimage.2008.03.037.

Ellegood, J., E. Anagnostou, B. A. Babineau, et al. 2015. "Clustering Autism: Using Neuroanatomical Differences in 26 Mouse Models to Gain Insight Into the Heterogeneity." *Molecular Psychiatry* 20, no. 1: 118–125. https://doi.org/10.1038/mp.2014.98.

Ellegood, J., A. Beauchamp, Y. Yee, et al. 2025. "Assigning Targetable Molecular Pathways to Transdiagnostic Subgroups Across Autism and Related Neurodevelopmental Disorders." *bioRxiv [Preprint]*. https://doi.org/10.1101/2025.03.04.641443.

Ellegood, J., J. P. Lerch, and R. M. Henkelman. 2011. "Brain Abnormalities in a Neuroligin3 R451C Knockin Mouse Model Associated With Autism." *Autism Research* 4, no. 5: 368–376. https://doi.org/10.1002/aur.215.

Ellingford, R., M. Tojo, A. Basson, and L. Andreae. 2024. "Male-Dominant Effects of Chd8 Haploinsufficiency on Synaptic Phenotypes During Development in Mouse Prefrontal Cortex." *ACS Chemical Neuroscience* 15: 1635–1642.

Garrido, D., S. Beretta, S. Grabrucker, et al. 2022. "Shank2/3 Double Knockout-Based Screening of Cortical Subregions Links the Retrosplenial Area to the Loss of Social Memory in Autism Spectrum Disorders." *Molecular Psychiatry* 27, no. 12: 4994–5006. https://doi.org/10.1038/s41380-022-01756-8.

Genovese, C. R., N. A. Lazar, and T. Nichols. 2002. "Thresholding of Statistical Maps in Functional Neuroimaging Using the False Discovery Rate." *NeuroImage* 15, no. 4: 870–878. https://doi.org/10.1006/nimg.2001.1037.

Gibbons, R. J., and D. R. Higgs. 2000. "Molecular-Clinical Spectrum of the ATR-X Syndrome." *American Journal of Medical Genetics* 97, no. 3: 204–212. https://doi.org/10.1002/1096-8628(200023)97:3<204::AID-AJMG1038>3.0.CO;2-X.

Gibbons, R. J., T. Wada, C. A. Fisher, et al. 2008. "Mutations in the Chromatin-Associated Protein ATRX." *Human Mutation* 29, no. 6: 796–802. https://doi.org/10.1002/humu.20734.

Goebbels, S., I. Bormuth, U. Bode, O. Hermanson, M. H. Schwab, and K.-A. Nave. 2006. "Genetic Targeting of Principal Neurons in Neocortex and Hippocampus of NEX-Cre Mice." *Genesis* 44, no. 12: 611–621. https://doi.org/10.1002/dvg.20256.

Ha, S., I.-J. Sohn, N. Kim, H. J. Sim, and K.-A. Cheon. 2015. "Characteristics of Brains in Autism Spectrum Disorder: Structure, Function and Connectivity Across the Lifespan." *Experimental Neurobiology* 24, no. 4: 273–284. https://doi.org/10.5607/en.2015.24.4.273.

Hahn, B., B. M. Robinson, C. J. Leonard, S. J. Luck, and J. M. Gold. 2018. "Posterior Parietal Cortex Dysfunction Is Central to Working Memory Storage and Broad Cognitive Deficits in Schizophrenia." *Journal of Neuroscience* 38, no. 39: 8378–8387. https://doi.org/10.1523/JNEUROSCI.0913-18.2018.

Haida, O., T. Al Sagheer, A. Balbous, et al. 2019. "Sex-Dependent Behavioral Deficits and Neuropathology in a Maternal Immune Activation Model of Autism." *Translational Psychiatry* 9, no. 1: 124. https://doi.org/10.1038/s41398-019-0457-y.

Hampson, D. R., and G. J. Blatt. 2015. "Autism Spectrum Disorders and Neuropathology of the Cerebellum." *Frontiers in Neuroscience* 9: 420.

Hollander, E., E. Anagnostou, W. Chaplin, et al. 2005. "Striatal Volume on Magnetic Resonance Imaging and Repetitive Behaviors in Autism." *Biological Psychiatry* 58, no. 3: 226–232. https://doi.org/10.1016/j.biopsych.2005.03.040.

Hong, S. J., S. L. Valk, A. Di Martino, M. P. Milham, and B. C. Bernhardt. 2018. "Multidimensional Neuroanatomical Subtyping of Autism Spectrum Disorder." *Cerebral Cortex* 28, no. 10: 3578–3588. https://doi.org/10.1093/cercor/bhx229.

Jung, H., H. Park, Y. Choi, et al. 2018. "Sexually Dimorphic Behavior, Neuronal Activity, and Gene Expression in Chd8-Mutant Mice." *Nature Neuroscience* 21, no. 9: 1218–1228. https://doi.org/10.1038/s41593-018-0208-z.

Kelly, E., F. Meng, H. Fujita, et al. 2020. "Regulation of Autism-Relevant Behaviors by Cerebellar–Prefrontal Cortical Circuits." *Nature Neuroscience* 23, no. 9: 1102–1110.

Lerch, J. P., J. B. Carroll, S. Spring, et al. 2008. "Automated Deformation Analysis in the YAC128 Huntington Disease Mouse Model." *NeuroImage* 39, no. 1: 32–39. https://doi.org/10.1016/j.neuroimage.2007.08.033.

Lerch, J. P., J. G. Sled, and R. M. Henkelman. 2011. "MRI Phenotyping of Genetically Altered Mice." In *Methods in Molecular Biology*, edited by M. Modo and J. Bulte, vol. 711, 349–361. Humana Press. https://doi.org/10.1007/978-1-61737-992-5_17.

Liu, G., L. Shi, J. Qiu, and W. Lu. 2022. "Two Neuroanatomical Subtypes of Males With Autism Spectrum Disorder Revealed Using Semi-Supervised Machine Learning." *Molecular Autism* 13, no. 1: 9. https://doi.org/10.1186/s13229-022-00489-3.

Mapelli, L., T. Soda, E. D'Angelo, and F. Prestori. 2022. "The Cerebellar Involvement in Autism Spectrum Disorders: From the Social Brain to Mouse Models." *International Journal of Molecular Sciences* 23, no. 7: 3894. https://doi.org/10.3390/ijms23073894.

Martin-Kenny, N., and N. G. Bérubé. 2020. "Effects of a Postnatal Atrx Conditional Knockout in Neurons on Autism-Like Behaviours in Male and Female Mice." *Journal of Neurodevelopmental Disorders* 12, no. 1: 17. https://doi.org/10.1186/s11689-020-09319-0.

Mo, A., E. A. Mukamel, F. P. Davis, et al. 2015. "Epigenomic Signatures of Neuronal Diversity in the Mammalian Brain." *Neuron* 86, no. 6: 1369–1384. https://doi.org/10.1016/j.neuron.2015.05.018.

Napolitano, A., S. Schiavi, P. La Rosa, et al. 2022. "Sex Differences in Autism Spectrum Disorder: Diagnostic, Neurobiological, and

Behavioral Features." *Frontiers in Psychiatry* 13: 889636. https://doi.org/10.3389/fpsyt.2022.889636.

Nieman, B. J., A. M. Flenniken, S. L. Adamson, R. M. Henkelman, and J. G. Sled. 2006. "Anatomical Phenotyping in the Brain and Skull of a Mutant Mouse by Magnetic Resonance Imaging and Computed Tomography." *Physiological Genomics* 24, no. 2: 154–162. https://doi.org/10.1152/physiolgenomics.00217.2005.

Qiu, L. R., D. J. Fernandes, K. U. Szulc-Lerch, et al. 2018. "Mouse MRI Shows Brain Areas Relatively Larger in Males Emerge Before Those Larger in Females." *Nature Communications* 9, no. 1: 2615. https://doi.org/10.1038/s41467-018-04921-2.

Quesnel, K., N. Martin-Kenny, and N. Berube. 2023. "A Mouse Model of ATRX Deficiency With Cognitive Deficits and Autistic Traits." *Journal of Neurodevelopmental Disorders* 15, no. 1: 39.

Richards, K., C. Watson, R. F. Buckley, et al. 2011. "Segmentation of the Mouse Hippocampal Formation in Magnetic Resonance Images." *NeuroImage* 58, no. 3: 732–740. https://doi.org/10.1016/j.neuroimage.2011.06.025.

Rowland, M. E., Y. Jiang, S. Shafiq, et al. 2023. "Systemic and Intrinsic Functions of ATRX in Glial Cell Fate and CNS Myelination in Male Mice." *Nature Communications* 14, no. 1: 7090. https://doi.org/10.1038/s41467-023-42752-y.

Sack, A. T. 2009. "Parietal Cortex and Spatial Cognition." *Behavioural Brain Research* 202, no. 2: 153–161. https://doi.org/10.1016/j.bbr.2009.03.012.

Sathyanesan, A., J. Zhou, J. Scafidi, D. H. Heck, R. V. Sillitoe, and V. Gallo. 2019. "Emerging Connections Between Cerebellar Development, Behaviour and Complex Brain Disorders." *Nature Reviews Neuroscience* 20, no. 5: 298–313. https://doi.org/10.1038/s41583-019-0152-2.

Saxena, K., L. Tamm, A. Walley, et al. 2012. "A Preliminary Investigation of Corpus Callosum and Anterior Commissure Aberrations in Aggressive Youth With Bipolar Disorders." *Journal of Child and Adolescent Psychopharmacology* 22, no. 2: 112–119. https://doi.org/10.1089/cap.2011.0063.

Singh, G., V. Singh, and J. S. Schneider. 2019. "Post-Translational Histone Modifications and Their Interaction With Sex Influence Normal Brain Development and Elaboration of Neuropsychiatric Disorders." *Biochimica et Biophysica Acta - Molecular Basis of Disease* 1865, no. 8: 1968–1981. https://doi.org/10.1016/j.bbadis.2018.10.016.

Steadman, P. E., J. Ellegood, K. U. Szulc, et al. 2014. "Genetic Effects on Cerebellar Structure Across Mouse Models of Autism Using a Magnetic Resonance Imaging Atlas." *Autism Research* 7, no. 1: 124–137. https://doi.org/10.1002/aur.1344.

Tamming, R. J., V. Dumeaux, Y. Jiang, et al. 2020. "Atrx Deletion in Neurons Leads to Sexually Dimorphic Dysregulation of miR-137 and Spatial Learning and Memory Deficits." *Cell Reports* 31, no. 13: 107838. https://doi.org/10.1016/j.celrep.2020.107838.

Tamming, R. J., J. R. Siu, Y. Jiang, M. A. M. Prado, F. Beier, and N. G. Berube. 2017. "Mosaic Expression of Atrx in the Mouse Central Nervous System Causes Memory Deficits." *Disease Models & Mechanisms* 10, no. 2: 119–126. https://doi.org/10.1242/dmm.027482.

Thakkar, K. N., F. E. Polli, R. M. Joseph, et al. 2008. "Response Monitoring, Repetitive Behaviour and Anterior Cingulate Abnormalities in Autism Spectrum Disorders (ASD)." *Brain* 131, no. Pt 9: 2464–2478. https://doi.org/10.1093/brain/awn099.

Tsumagari, K., Y. Sato, H. Aoyagi, H. Okano, and J. Kuromitsu. 2023. "Proteomic Characterization of Aging-Driven Changes in the Mouse Brain by Co-Expression Network Analysis." *Scientific Reports* 13, no. 1: 18191. https://doi.org/10.1038/s41598-023-45570-w.

Ullmann, J. F. P., C. Watson, A. L. Janke, N. D. Kurniawan, and D. C. Reutens. 2013. "A Segmentation Protocol and MRI Atlas of the C57BL/6J Mouse Neocortex." *NeuroImage* 78: 196–203. https://doi.org/10.1016/j.neuroimage.2013.04.008.

Wada, T., H. Ban, M. Matsufuji, et al. 2013. "Neuroradiologic Features in α-Linked α-Thalassemia/Mental Retardation Syndrome." *American Journal of Neuroradiology* 34, no. 10: 2034–2038. https://doi.org/10.3174/ajnr.A3560.

Yee, Y., J. Ellegood, L. French, and J. P. Lerch. 2024. "Organization of Thalamocortical Structural Covariance and a Corresponding 3D Atlas of the Mouse Thalamus." *NeuroImage* 285: 120453. https://doi.org/10.1016/j.neuroimage.2023.120453.

Zhang, D., B. Yu, J. Liu, et al. 2017. "Altered Visual Cortical Processing in a Mouse Model of MECP2 Duplication Syndrome." *Scientific Reports* 7, no. 1: 6468. https://doi.org/10.1038/s41598-017-06916-3.

Supporting Information

Additional supporting information can be found online in the Supporting Information section. **Figure S1:** Graphical representation of relative volumes of hippocampal subregions in male and female control and $Atrx^{NEXCre}$ mice. **Figure S2:** Graphical representation of relative volumes of cortical subregions in male and female control and $Atrx^{NEXCre}$ mice. **Figure S3:** Graphical representation of relative volumes of cerebellar subregions in male and female control and $Atrx^{NEXCre}$ mice. **Figure S4:** Representative images of brain regions showing NEXCre expressing cells labeled with SUN1-GFP and co-labeled with ATRX, demonstrating regions with ATRX loss vs. ATRX retained expression. **Data S1:** Raw MRI data. Excel file containing raw absolute volumes and relative volume outputs, as well as statistical analysis across all brain regions.